Nuclear Engineering and Technology 49 (2017) 1135–1142

Contents lists available at ScienceDirect

Nuclear Engineering and Technology

journal homepage: www.elsevier.com/locate/net

Technical Note

Acceleration of step and linear discontinuous schemes for the method of characteristics in DRAGON5

Alain Hébert

École Polytechnique de Montréal, P.O. Box 6079 Station "Centre-Ville", Montréal, Québec H3C 3A7, Canada

ARTICLE INFO

Article history:
Received 21 June 2017
Accepted 7 July 2017
Available online 25 July 2017

Keywords:
Method of characteristics
Linear discontinuous source
Algebraic collapsing acceleration
Generalized minimal residual acceleration method
DRAGON5 code

ABSTRACT

The applicability of the algebraic collapsing acceleration (ACA) technique to the method of characteristics (MOC) in cases with scattering anisotropy and/or linear sources was investigated. Previously, the ACA was proven successful in cases with isotropic scattering and uniform (step) sources. A presentation is first made of the MOC implementation, available in the DRAGON5 code. Two categories of schemes are available for integrating the propagation equations: (1) the first category is based on exact integration and leads to the classical step characteristics (SC) and linear discontinuous characteristics (LDC) schemes and (2) the second category leads to diamond differencing schemes of various orders in space. The acceleration of these MOC schemes using a combination of the generalized minimal residual [GMRES(m)] method preconditioned with the ACA technique was focused on. Numerical results are provided for a two-dimensional (2D) eight-symmetry pressurized water reactor (PWR) assembly mockup in the context of the DRAGON5 code.

1. Introduction

This paper is related to the application of the method of characteristics (MOC) for solving the neutron transport equation [1]. This method iteratively solves the transport equation in terms of the angular moments of regional fluxes by summation upon a tracking. Solution of the characteristics form of the transport equation is performed over each track as a function of a polynomial approximation for the neutron source along this track. Most production implementations of the MOC are based either on a discontinuous flat-source spatial approximation [2–7] or on a discontinuous linear-source spatial approximation [8–14] along the tracks. We investigated a new class of linear characteristics schemes along cyclic tracks for solving the transport equation for neutral particles with scattering anisotropy. These algorithms rely on step and linear discontinuous exact integration, as described in [15,16]. These schemes are based on linear discontinuous coefficients that are derived through the application of approximations describing the mesh-averaged spatial flux moments in terms of spatial source moments and of the beginning- and end-of-segment flux values. The linear discontinuous characteristics (LDC) scheme is inherently conservative, a property that facilitates its practical implementation and the acceleration of its scattering iterations in a production code such as DRAGON5 [17]. In this paper, the focus is on the acceleration of the scattering iterations which are required with the application of the MOC. Two acceleration techniques are investigated: (1) the generalized minimal residual [GMRES(m)] method [18] and (2) the algebraic collapsing acceleration (ACA) method [4]. The application of these techniques was demonstrated on a two-dimensional (2D) eight-symmetry pressurized water reactor (PWR) assembly mockup in the context of the DRAGON5 code. It is shown that the acceleration remains effective in spite of the introduction of scattering anisotropy and linear sources.

2. Theory

A brief introduction of the MOC formalism is given. The boundary conditions treatment along with the details on the iterative strategy are not reported in the present paper but can be found in [1]. The classical step characteristics (SC) and flat-source diamond differencing (DD0) schemes are also presented in this book. Emphasis is put on the characteristic form of the transport equation which arises from the trajectory-based formulation of the flux integration. The conservation principle is formulated within this framework.

The backward characteristic form of the transport was obtained in Section 3.2.1 of [1]. The one-speed and steady-state form of this equation is written as:

E-mail address: alain.hebert@polymtl.ca.

http://dx.doi.org/10.1016/j.net.2017.07.004

$$\frac{d}{ds}\phi(r+s\,\Omega,\Omega)+\Sigma(r+s\,\Omega)\,\phi(r+s\,\Omega,\Omega)=Q(r+s\,\Omega,\Omega) \tag{1}$$

where r is the starting point of the particle, s is the distance travelled by the particle on its characteristic, Ω is the direction of the characteristic, $\Sigma(r)$ is the value of the macroscopic total cross section at r, $\varphi(r,\Omega)$ is the particle angular flux at r, and $Q(r,\Omega)$ is the fixed source at r.

The spatial integration domain is partitioned into regions of volume $\{V_i; i=1,I\}$, each of them characterized by uniform nuclear properties and surrounded by boundary surfaces $\{S_\alpha;\alpha=1,\Lambda\}$. The MOC is based on the discretization of Eq. (1) along each path of the particle and on the integration of the flux contributions using spatial integrals of the form:

$$\begin{aligned}V_i\phi_i &= \int_{V_i} d^3r \int_{4\pi} d^2\Omega\;\phi(r,\Omega)\\ &= \int_Y d^4T \int_{-\infty}^{\infty} ds\;\chi_{V_i}(T,s)\;\phi(p+s\Omega,\Omega)\end{aligned} \tag{2}$$

where φ_i is the average flux in region i and $\mathrm{Y}=(T)$ is the tracking domain.

A single characteristic T is determined by its orientation Ω and its starting point p defined on a reference plane Π_Ω perpendicular to T, as depicted in Fig. 1. The characteristics are selected in domain $Y=4\pi\times\Pi_\Omega$ which is characterized by an order-four differential $d^4T=d^2\Omega\,d^2p$. The local coordinate s defines the distance of point r with respect to plane Π_Ω. Finally, the characteristic function $\chi_{V_i}(T,s)=1$ if point $p+s\Omega$ of characteristic T is located inside V_i, and 0 otherwise.

The MOC requires knowledge of region indices N_k and segment lengths ℓ_k describing the overlapping of characteristic T with the domain. This information is written $(N_k,\ell_k;k=1,K)$ where K is the total number of regions crossed by T. It is important to note that segment lengths ℓ_k are always defined in three-dimensions, even for prismatic 2D geometries. The intersection points of a characteristic with the region boundaries, and the corresponding angular flux on these boundaries, are written:

$$r_{k+1}=r_k+\ell_k\,\Omega;\quad k=1,K. \tag{3}$$

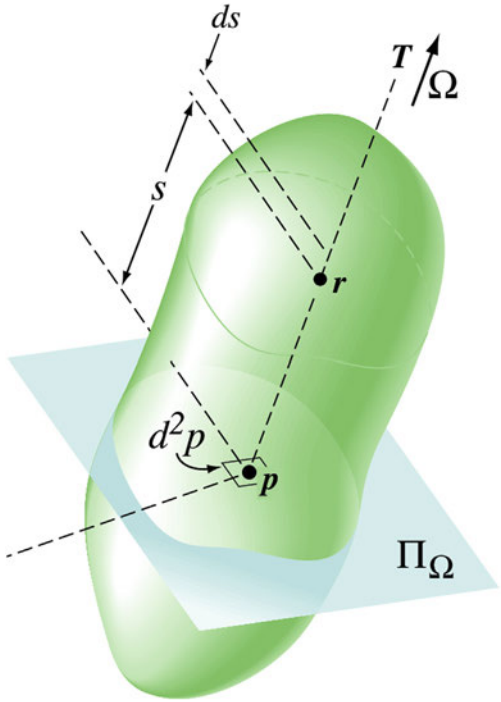

Fig. 1. Spatial integration domain.

2.1. The linear discontinuous characteristic assumption in space

A linear representation of the sources along characteristic T based on an expansion in normalized Legendre polynomials is introduced. This expansion is applied over segment $\ell_k(T)$, as pictured in Fig. 2. Its mathematical expression is:

$$Q(r_k+s\,\Omega,\Omega)=Q_k^{(0)}(\Omega)+2\sqrt{3}\left[s-\frac{\ell_k(T)}{2}\right]Q_k^{(1)}(\Omega);\quad k=1,K \tag{4}$$

where

$$Q_k^{(0)}(\Omega)=\frac{1}{\ell_k(T)}\int_0^{\ell_kT} ds\;Q(r_k+s\,\Omega,\Omega) \tag{5}$$

and

$$Q_k^{(1)}(\Omega)=\frac{2\sqrt{3}}{\ell_k^3(T)}\int_0^{\ell_kT} ds\left[s-\frac{\ell_k(T)}{2}\right]Q(r_k+s\,\Omega,\Omega). \tag{6}$$

Knowledge of the moments of the flux over segment $\ell_k(T)$ are required in order to compute components of the source, $Q_k^{(0)}(\Omega)$ and $Q_k^{(1)}(\Omega)$. The moments of the segment-averaged fluxes are defined as:

$$\overline{\phi}_k^{(0)}(T)=\frac{1}{\ell_k(T)}\int_0^{\ell_kT} ds\;\phi(r_k+s\,\Omega,\Omega) \tag{7}$$

and

$$\overline{\phi}_k^{(1)}(T)=\frac{2\sqrt{3}}{\ell_k^3(T)}\int_0^{\ell_kT} ds\left[s-\frac{\ell_k(T)}{2}\right]\phi(r_k+s\,\Omega,\Omega). \tag{8}$$

Substitution of the linear source approximation Eq. (4) into the characteristics form of the transport equation leads to:

$$\begin{aligned}&\frac{d}{ds}\phi(r_k+s\,\Omega,\Omega)+\Sigma_{N_k}\phi(r_k+s\,\Omega,\Omega)\\ &\quad=Q_k^{(0)}(\Omega)+2\sqrt{3}\left[s-\frac{\ell_k(T)}{2}\right]Q_k^{(1)}(\Omega).\end{aligned} \tag{9}$$

Analytical solution of Eq. (9) is written:

$$\begin{aligned}\phi(r_k+s\,\Omega,\Omega)=\phi(r_k,\Omega)\,\mathrm{e}^{-s\,\Sigma_{N_k}}&+\frac{Q_k^{(0)}(\Omega)}{\Sigma_{N_k}}\left(1-\mathrm{e}^{-s\,\Sigma_{N_k}}\right)\\ &+\frac{\sqrt{3}\,Q_k^{(1)}(\Omega)}{\Sigma_{N_k}^2}\left[2\mathrm{e}^{-s\,\Sigma_{N_k}}+2\left(s\,\Sigma_{N_k}-1\right)\right.\\ &\left.-\Sigma_{N_k}\ell_k(T)\left(1-\mathrm{e}^{-s\,\Sigma_{N_k}}\right)\right].\end{aligned} \tag{10}$$

where $\phi_k(T)=\phi(r_k,\Omega)$.

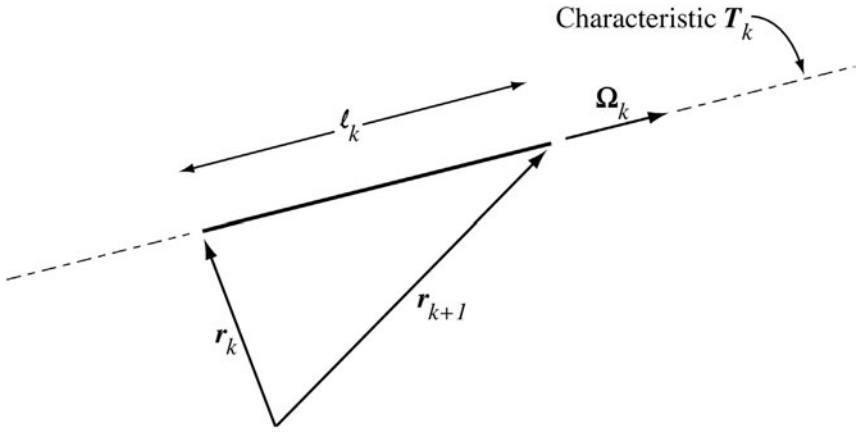

Fig. 2. A segment of a single characteristic.

Using Eq. (7), it is possible to rewrite Eq. (2) as:

$$V_i \phi_i^{(0)} = \int_Y d^4T \sum_k \delta_{iN_k} \ell_k(T) \overline{\phi}_k^{(0)}(T) \tag{11}$$

where δ_{ij} is the Kronecker delta function and where the summation over k is performed over all the existing indices. All the characteristics T are spanned in Eq. (11), but only those that effectively cross region i contribute to the integral. We introduced a summation over characteristics with index $n \leq N$, with N as the total number of characteristics. Note that each track of the tracking object is used twice as two characteristics, in Ω_n and $-\Omega_n$ directions.

Using the same approach that leads to Eq. (11), the volume of region i is written:

$$4\pi V_i = \int_Y d^4T \sum_k \delta_{iN_k} \ell_k(T). \tag{12}$$

Eq. (12) is the numerical approximation used in MOC for the numerical volumes. The effect of this approximation can be mitigated by renormalizing tracking in order to force the equality. Two renormalization options are available, depending if the normalization factors are function or not of the track directions.

Setting $\phi_k(T) \equiv \phi(r_k, \Omega)$ and $\phi_{k+1}(T) \equiv \phi\ (r_k + \ell_k(T\,\Omega, \Omega)$, it is possible to write the propagation equations for the MOC with linear source approximation and anisotropic scattering as:

$$\phi_{k+1}(T) = A_k(T)\,\phi_k(T) + B_k(T)\,Q_k^{(0)}(\Omega) + C_k(T)\,\ell_k(T)\,Q_k^{(1)}(\Omega)$$

$$\overline{\phi}_k^{(0)}(T) = \frac{1}{\ell_k(T)}\Big[B_k(T)\,\phi_k(T) + D_k(T)\,Q_k^{(0)}(\Omega) + E_k(T)\,\ell_k(T)\,Q_k^{(1)}(\Omega)\Big]$$

and

$$\overline{\phi}_k^{(1)}(T) = \frac{1}{\ell_k(T)^2}\Big[F_k(T)\,\phi_k(T) + G_k(T)\,Q_k^{(0)}(\Omega) + H_k(T)\,\ell_k(T)\,Q_k^{(1)}(\Omega)\Big] \tag{13}$$

where the set of coefficients $A_k(T)$–$H_k(T)$ can take different values, depending on the type of MOC approximation and on the magnitude of the optical path $\tau_k(T)$. The set of coefficient corresponding to the linear discontinuous characteristics (LDC) case with $\tau_k(T) \geq \varepsilon$ is:

$$A_k(T) = \mathrm{e}^{-\tau_k(T)}$$

$$B_k(T) = \frac{1}{\Sigma_{N_k}}\left(1 - \mathrm{e}^{-\tau_k(T)}\right)$$

$$C_k(T) = \frac{\sqrt{3}}{\tau_k(T)\,\Sigma_{N_k}}\left(2\mathrm{e}^{-\tau_k(T)} + \tau_k(T) - 2 + \tau_k(T)\,\mathrm{e}^{-\tau_k(T)}\right)$$

$$D_k(T) = \frac{\ell_k(T)}{\Sigma_{N_k}}\left(1 - \frac{1 - \mathrm{e}^{-\tau_k(T)}}{\tau_k(T)}\right)$$

$$E_k(T) = -\frac{\sqrt{3}}{\tau_k(T)\,\Sigma_{N_k}^2}\left(2\mathrm{e}^{-\tau_k(T)} + \tau_k(T) - 2 + \tau_k(T)\,\mathrm{e}^{-\tau_k(T)}\right)$$

$$F_k(T) = -\frac{\sqrt{3}}{\tau_k(T)\Sigma_{N_k}}\left(2\mathrm{e}^{-\tau_k(T)} + \tau_k(T) - 2 + \tau_k(T)\,\mathrm{e}^{-\tau_k(T)}\right)$$

$$G_k(T) = \frac{\sqrt{3}}{\tau_k(T)\Sigma_{N_k}^2}\left(2\mathrm{e}^{-\tau_k(T)} + \tau_k(T) - 2 + \tau_k(T)\,\mathrm{e}^{-\tau_k(T)}\right)$$

$$G_k(T) = \frac{\sqrt{3}}{\tau_k(T)\Sigma_{N_k}^2}\left(2\mathrm{e}^{-\tau_k(T)} + \tau_k(T) - 2 + \tau_k(T)\mathrm{e}^{-\tau_k(T)}\right)$$

$$H_k(T) = \frac{1}{\tau_k(T)^2\,\Sigma_{N_k}^2}\Big[12 - 12\mathrm{e}^{-\tau_k(T)} - 3\tau_k(T)^2 + \tau_k(T)^3 - 3\tau_k(T)^2\mathrm{e}^{-\tau_k(T)} - 12\tau_k(T)\mathrm{e}^{-\tau_k(T)}\Big]. \tag{14}$$

Otherwise, in case of a small optical path, Taylor expansions of the above relations are used.

Solution of Eq (13) over a finite track is straightforward. Each track is travelled back and forth starting from the initial boundary where $\phi_1(T)$ or $\phi_{K+1}(-T)$ is set. This approach is simpler than the algorithm proposed in [15], but leads to the same solution.

Solution of Eq. (13) over a cyclic track is based on the requirement that $\phi_{K+1}(T) = \phi_1(T)$ where K is the total number of segments in all the subtracks constituting the track T. A recursion is applied, as described in [16].

2.2. Determination of the spherical harmonics coefficients

Expressions of the segment-averaged fluxes $\overline{\phi}_k^{(0)}(T_n)$ and $\overline{\phi}_k^{(1)}(T_n)$ are expanded in spherical harmonics. The uniform component of the flux in direction Ω_n for the track T_n is defined as:

$$\overline{\phi}_k^{(0)}(T_n) = \sum_{\ell=0}^{\infty} \frac{2\ell+1}{4\pi} \sum_{\substack{m=-\ell \\ \ell+m \text{ even}}}^{\ell} \overline{\phi}_{\ell,k}^m R_\ell^m(\Omega_n) \tag{15}$$

and the linear component of the flux in direction Ω_n for the track T_n is defined from its Cartesian components as:

$$\overline{\phi}_k^{(1)}(T_n) = \sum_{\ell=0}^{\infty} \frac{2\ell+1}{4\pi} \sum_{\substack{m=-\ell \\ \ell+m \text{ even}}}^{\ell} \left[\nabla \overline{\phi}_{\ell,k}^m \cdot \Omega\right] R_\ell^m(\Omega_n). \tag{16}$$

Here, important remarks should be made concerning Eqs. (15) and (16). We are not assuming limited expansions for $\overline{\phi}_k^{(0)}(T_n)$ and $\overline{\phi}_k^{(1)}(T_n)$ Eqs. (15) and (16) are introduced as a convenient way to define the flux moments $\overline{\phi}_{\ell,k}^m$ and $\nabla\overline{\phi}_{\ell,k}^m$ that need to be evaluated up to the order of the anisotropic source. Angular accuracy of the flux is limited by the number of discrete angles used in the tracking, not by a limited spherical harmonic expansion. Finally, we assume a 2D geometry, so that only even $l+m$ indices are used and so that flux moments $\nabla\overline{\phi}_{\ell,k}^m$ are two-component vectors. The high-order property of our characteristics scheme in space comes from the introduction of Eq. (16).

Two conditions have to be fulfilled in order for the MOC scheme to be inherently conservative: (1) the balance equation must be imposed on each track; and (2) consistent spherical harmonic moments must be defined for $\overline{\phi}_{\ell,k}^m$ and $\nabla\overline{\phi}_{\ell,k}^m$ in Eqs. (15) and (16). This second condition is more difficult to reach for the LDC and DD1 schemes, due to the nonorthogonality of the spherical harmonic basis $\Omega\, R_\ell^m(\Omega)$.

Eq. (15) is a plain spherical harmonic expansion. Its segment-averaged coefficients are therefore written:

$$\overline{\phi}_{\ell,k}^m = \int_{4\pi} d^2\Omega\, R_\ell^m(\Omega)\, \overline{\phi}_k^{(0)}(T_n) \;\; ; \quad \ell \le L \tag{17}$$

and can be collapsed into region-averaged spherical harmonic moment ϕ_{ℓ,N_k}^m, where N_k is the region index containing segment k.

The determination of coefficients $\nabla\phi_{\ell,N_k}^m \equiv \text{col}\left(\frac{\partial}{\partial x}\phi_{\ell,N_k}^m, \frac{\partial}{\partial y}\phi_{\ell,N_k}^m\right)$ is now presented. Unfortunately, the trial functions $\Omega\, R_\ell^m(\Omega)$ are not mutually orthogonal. Off-diagonal contributions need to be taken into account. As presented in [15], the spherical harmonics coefficients ψ_{ℓ,N_k}^m are a linear combination of the slope components $\nabla\phi_{\ell,N_k}^m$. The MOC procedure proceed in successive steps:

(1) Based on Eq. (17), sum the angular neutron flux segment-averaged contributions over volumes V_i and smear these contributions over computational regions. This relation is written:

$$\frac{1}{4\pi}\phi_{\ell,i}^m = \frac{\sum_{n=1}^N \omega_n \sum_k \delta_{iN_k}\, \wp_k(T_n)\, \overline{\phi}_k^{(0)}(T_n)\, R_\ell^m(\Omega_n)}{\sum_{n=1}^N \omega_n \sum_k \delta_{iN_k}\, \wp_k(T_n)} \tag{18}$$

where the segment-averaged flux $\overline{\phi}_k^{(0)}(T_n)$ can be evaluated from the propagation Eq. (13). In the context of the LDC and DD1 schemes, Eq. (18) is still used, in conjunction with Eq. (13). The basic relation allowing MOC to construct the slope-related moments $\overline{\varphi}_{\ell,i}^m$ is obtained from a relation similar to Eq. (17), using trial functions $R_\ell^m(\Omega_n)\,\Omega_n$, and written:

$$\overline{\varphi}_{\ell,k}^m = \int_{4\pi} d^2\Omega\, \Omega\, R_\ell^m(\Omega)\, \overline{\phi}_k^{(1)}(T_n). \tag{19}$$

Smearing these contributions over computational regions, we obtain:

$$\frac{1}{4\pi}\psi_{\ell,i}^m = \frac{\sum_{n=1}^N \omega_n \sum_k \delta_{iN_k}\, \wp_k(T_n)\, \overline{\phi}(T_n)\, R_\ell^m(\Omega_n)\, \Omega_n}{\sum_{n=1}^N \omega_n \sum_k \delta_{iN_k}\, \wp_k(T_n)} \tag{20}$$

where smeared values $\psi_{\ell,i}^m$ are evaluated up to order $L+2$.

(2) The spherical harmonics expansion of the flux gradient on volume i is based on Eq. (16):

$$\phi_i^{(1)}(\Omega) = \sum_{\ell'=0}^{\infty} \frac{2\ell'+1}{4\pi} \sum_{\substack{m'=-\ell' \\ \ell'+m' \text{ even}}}^{\ell'} \left[\nabla\phi_{\ell',i}^{m'} \cdot \Omega\right] R_{\ell'}^{m'}(\Omega). \tag{21}$$

We multiply both sides by $\Omega R_\ell^m(\Omega)$ and integrates over 4π:

$$\psi_{\ell,i}^m = \sum_{\ell'=0}^{\infty} \frac{2\ell'+1}{4\pi} \sum_{\substack{m'=-\ell' \\ \ell'+m' \text{ even}}}^{\ell'} \int_{4\pi} d^2\Omega\, \Omega\, R_\ell^m(\Omega) \times \left(\nabla\phi_{\ell',i}^{m'} \cdot \Omega\right) R_{\ell'}^{m'}(\Omega) \tag{22}$$

where

$$\psi_{\ell,i}^m = \int_{4\pi} d^2\Omega\, \Omega\, R_\ell^m(\Omega)\phi_i^{(1)}(\Omega). \tag{23}$$

Eq. (22) is the relation between slope components $\nabla\phi_{\ell,i}^m$ and smeared values $\psi_{\ell,i}^m$ obtained from Eq. (20).

(3) Slope components $\nabla\phi_{\ell,i}^m$ in each region i are obtained by inverting Eq. (22), which can be rewritten as [15]:

$$\psi_{\ell,i}^m = \sum_{\ell'=0}^{L+2} \frac{2\ell'+1}{4\pi} \sum_{\substack{m'=-\ell' \\ \ell'+m' \text{ even}}}^{\ell'} \mathrm{M}_{\ell,\ell'}^{m,m'} \cdot \nabla\phi_{\ell',i}^{m'} \tag{24}$$

where $\ell \le L+2$ and where the dyadic coefficients are written:

$$\mathrm{M}_{\ell,\ell'}^{m,m'} = \int_{4\pi} d^2\Omega\, (\Omega \otimes \Omega)\, R_\ell^m(\Omega)\, R_{\ell'}^{m'}(\Omega). \tag{25}$$

Only a 2×2 submatrix of $\mathrm{M}_{\ell,\ell'}^{m,m'}$ is worthwhile to analyze 2D geometries, based on the following definition of:

$$\Omega \otimes \Omega = \begin{bmatrix} R_1^1(\Omega)R_1^1(\Omega) & R_1^1(\Omega)R_1^{-1}(\Omega) \\ R_1^1(\Omega)R_1^{-1}(\Omega) & R_1^{-1}(\Omega)R_1^{-1}(\Omega) \end{bmatrix}. \tag{26}$$

Calculation of coefficients $\mathrm{M}_{\ell,\ell'}^{m,m'}$ up to order P_3 is presented in [15]. In the simple case of isotropic scattering sources, moments $\psi_{0,i}^0$ are a linear combination of slope components $\nabla\phi_{0,i}^0$ and $\nabla\phi_{2,i}^m$. After

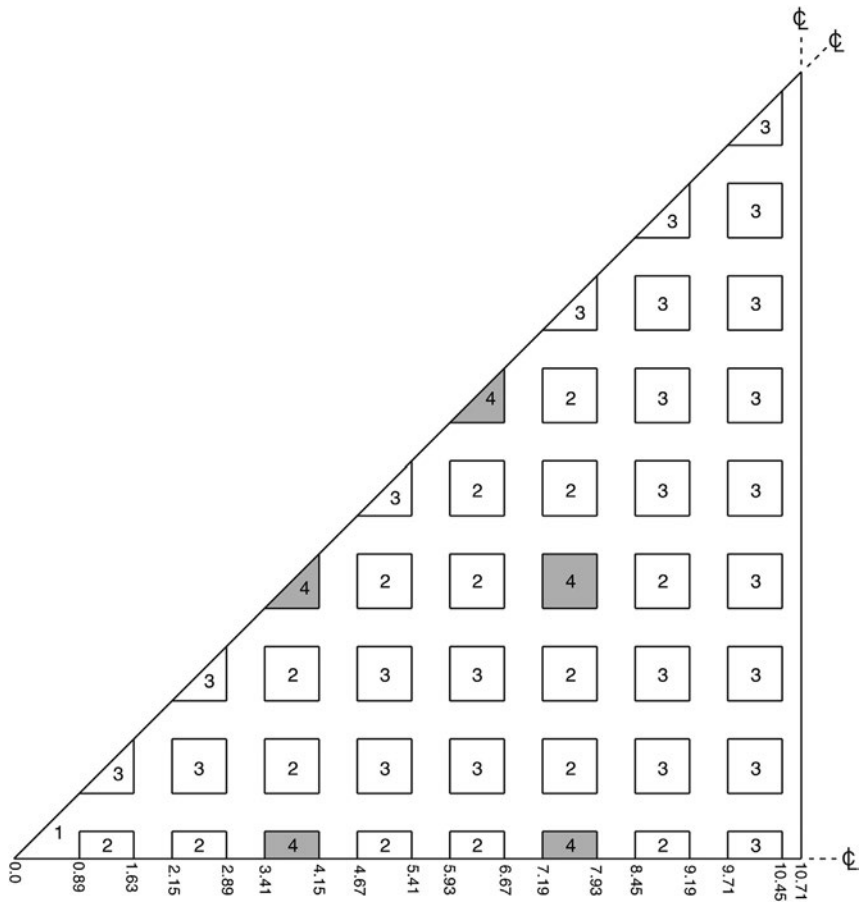

Fig. 3. Description of the AIC assembly benchmark. The dimensions are given in cm. AIC, silver–indium–cadmium.

inversion of Eq. (24), calculation of $\nabla\phi^0_{0,i}$ requires knowledge of $\psi^0_{0,i}$ and $\psi^m_{2,i}$. This procedure is required for making the LDC and DD1 schemes inherently conservative.

We should also remember an important issue presented in a recent study [15]. There is an inherent singularity with the linear coefficients of Eq. (24) at each Legendre order with $\ell > 0$. It is therefore not possible to determine the moments of the flux gradient $\nabla\phi^m_{\ell,i}$ by performing a simple inversion of Eq. (24). The approach proposed in [15] consists of adding heuristic equations to the linear system and to perform a pseudoinversion of the resulting rectangular matrix. We have been able to find heuristic equations up to $\nabla\phi^m_{\ell,i}$ order.

(4) The last operation consists to compute the scattering sources for the next scattering iteration. An assumption is made on the anisotropy order L of the scattering sources. The uniform source in direction Ω_n is defined as:

$$Q^{(0)}_{N_k}(\Omega_n) = \sum_{\ell=0}^{L} \frac{2\ell+1}{4\pi} \sum_{\substack{m=-\ell \\ \ell+m \text{ even}}}^{\ell} Q^m_{\ell,N_k} R^m_\ell(\Omega_n). \tag{27}$$

The linear source in direction Ω_n is defined from its Cartesian components as:

$$Q^{(1)}_{N_k}(\Omega_n) = \sum_{\ell=0}^{L} \frac{2\ell+1}{4\pi} \sum_{\substack{m=-\ell \\ \ell+m \text{ even}}}^{\ell} \left(\nabla Q^m_{\ell,N_k} \cdot \Omega_n\right) R^m_\ell(\Omega_n) \tag{28}$$

The spherical harmonic moments of the sources are expressed as a function of fixed sources $S^m_{\ell,i}$ and scattering information as:

$$Q^m_{\ell,i} = S^m_{\ell,i} + \Sigma_{s,\ell,i}\, \phi^m_{\ell,i} \tag{29}$$

and

$$\nabla Q^m_{\ell,i} = \nabla S^m_{\ell,i} + \Sigma_{s,\ell,i} \nabla\phi^m_{\ell,i}\,. \tag{30}$$

2.3. Synthetic acceleration

The particle source distribution $Q(r,\Omega)$ appearing in the right-hand side of the transport Eq. (1) is written in terms of the within-group scattering reaction rate using:

$$Q(r,\Omega) = \sum_{\ell=0}^{L} \frac{2\ell+1}{4\pi} \sum_{m=-\ell}^{\ell} \left[\Sigma_{w,\ell}(r)\, \phi^m_\ell(r) + Q^{\diamond m}_\ell(r)\right] R^m_\ell(\Omega) \tag{31}$$

where $\Sigma_{w,\ell}(r)$ is the ℓ-th Legendre moment of the macroscopic within-group scattering cross section, $\Phi^m_\ell(r)$ is a spherical harmonic component of the flux and $Q^{\diamond m}_\ell(r)$ is a spherical harmonic component of the source representing other contributions such as fission and out-of-group scattering rates. Scattering source iterations are always required with the MOC. Introducing an iteration index (κ), the basic scattering source iterative scheme is written:

Table 1
MOC results for the AIC assembly benchmark with scattering anisotropy. Step characteristic (SC) scheme.[a]

Submesh	N_{tot}	k_{eff}	Δk_{eff} (pcm)	$\varepsilon_{\max}$ (%)	ε (%)	CPU (s)
1 + 1	513	0.908298	−654.1	2.35	0.54	2.4
2 + 4	3,978	0.913206	−163.3	0.60	0.16	7.0
3 + 6	9,009	0.914373	−46.6	0.24	0.06	10.4
4 + 8	15,759	0.914882	4.3	0.20	0.06	17.4

AIC, silver–indium–cadmium; MOC, method of characteristics; SC, step characteristic.
[a] Reference $k_{\text{eff}} = 0.914839$.

Table 2
MOC results for the AIC assembly benchmark with scattering anisotropy. Linear discontinuous characteristic (LDC) scheme.[a]

Submesh	N_{tot}	k_{eff}	Δk_{eff} (pcm)	$\varepsilon_{\max}$ (%)	$\bar{\varepsilon}$ (%)	CPU (s)
1 + 1	1,539	0.914345	−47.3	0.87	0.11	6.8
2 + 4	11,934	0.914397	−44.2	0.25	0.08	19.1

AIC, silver–indium–cadmium; LDC, linear discontinuous characteristic; MOC, method of characteristics.
[a] Reference $k_{\text{eff}} = 0.914839$. CPU stands for Central processing unit time.

$$\frac{d}{ds}\phi^{(\kappa+1)}(r+s\,\Omega,\Omega)+\Sigma(r+s\,\Omega)\phi^{(\kappa+1)}(r+s\,\Omega,\Omega) = \sum_{\ell=0}^{L}\frac{2\ell+1}{4\pi}\sum_{m=-\ell}^{\ell}\left[\Sigma_{w,\ell}(r+s\,\Omega)\phi_\ell^{m,(\kappa)}(r+s\,\Omega) + Q_\ell^{\diamond m}(r+s\,\Omega)\right]R_\ell^m(\Omega) \tag{32}$$

where $\Phi_\ell^{m,(\kappa)}(r)$ are the spherical harmonic flux component computed with the MOC at the (κ)-th iteration.

As pointed out in [19], the fixed-point convergence of Eq. (32) becomes difficult with large domains or in the presence of purely scattering media as the scattering ratio approaches one. In this case, Alcouffe [19] proposed a preconditioning known as synthetic acceleration, based on the following scheme:

$$\frac{d}{ds}\phi^{(\kappa+1/2)}(r+s\,\Omega,\Omega)+\Sigma(r+s\,\Omega)\phi^{(\kappa+1/2)}(r+s\,\Omega,\Omega) = \sum_{\ell=0}^{L}\frac{2\ell+1}{4\pi}\sum_{m=-\ell}^{\ell}\left[\Sigma_{w,\ell}(r+s\,\Omega)\phi_\ell^{m,(\kappa)}(r+s\,\Omega) + Q_\ell^{\diamond m}(r+s\,\Omega)\right]R_\ell^m(\Omega) \tag{33}$$

$$\Omega\cdot\nabla\delta\phi^{(\kappa+1/2)}(r,\Omega)+\Sigma(r)\delta\phi^{(\kappa+1/2)}(r,\Omega) - \frac{1}{4\pi}\Sigma_{w,0}(r)\delta\phi_0^{0,(\kappa+1/2)}(r)R_\ell^m(\Omega) = \frac{1}{4\pi}\Sigma_{w,0}(r)\left[\phi_0^{0,(\kappa+1/2)}(r)-\phi_0^{0,(\kappa)}(r)\right]R_\ell^m(\Omega) \tag{34}$$

and

$$\varphi^{(\kappa+1)}(r,\Omega)=\varphi^{(\kappa+1/2)}(r,\Omega)+\delta\varphi^{(\kappa+1/2)}(r,\Omega). \tag{35}$$

In the present work, Eq. (34) is a simplified transport equation with scattering isotropy and uniform (flat) sources. Moreover, we have chosen to solve this equation with the Algebraic Collapsing (AC) method, as presented in [4] and Section 3.10.3 of [1]. This choice is similar to the approach proposed by Alcouffe [19], consisting of replacing Eq. (34) by a form of the transport equation that is simpler to solve. In his work, Alcouffe proposed to replace Eq. (34) with a compatible diffusion equation, leading to the diffusion synthetic acceleration (DSA) scheme. A synthetic acceleration approach based on the AC method to solve Eq. (34) has been proposed and validated in the past, but only in cases where Eq. (33) is solved with the MOC with scattering isotropy and uniform (flat) sources [20]. The main contribution of this paper is to validate the use of a synthetic acceleration approach based on the AC method in cases with anisotropic scattering and linear sources.

3. Results

The SC and LDC schemes with scattering anisotropy have been implemented in the DRAGON5 lattice code for 2D problems. These implementations were validated on a set of simple few-group benchmarks in fundamental mode condition (i.e., with reflective

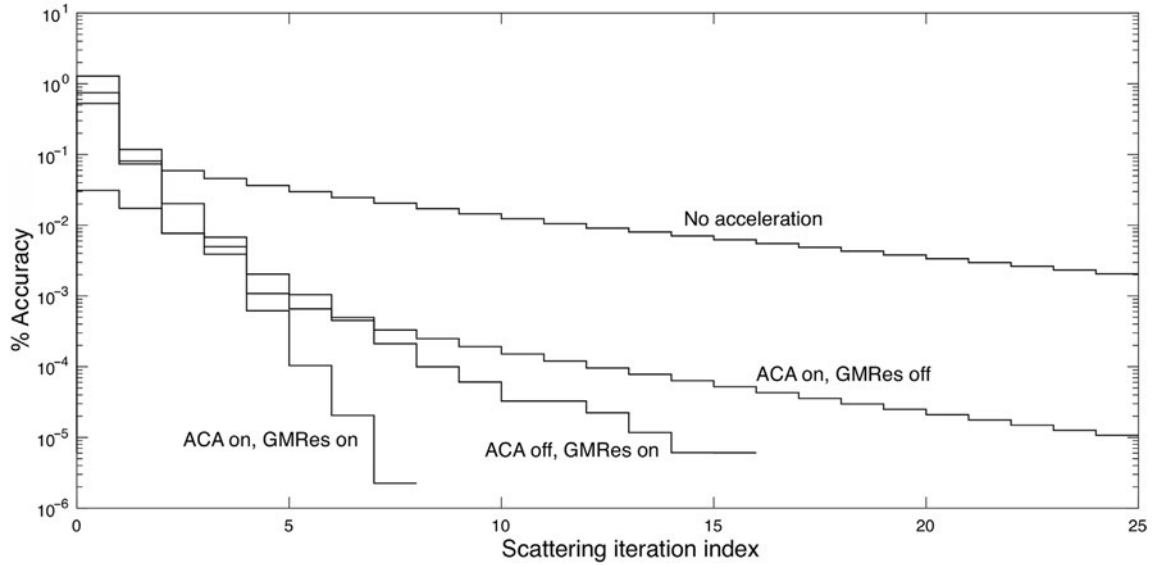

Fig. 4. Acceleration strategies for the MOC with SC scheme. Linear scattering anisotropy is present. ACA, algebraic collapsing acceleration; GMRES, generalized minimal residual; MOC, method of characteristics; SC, step characteristics.

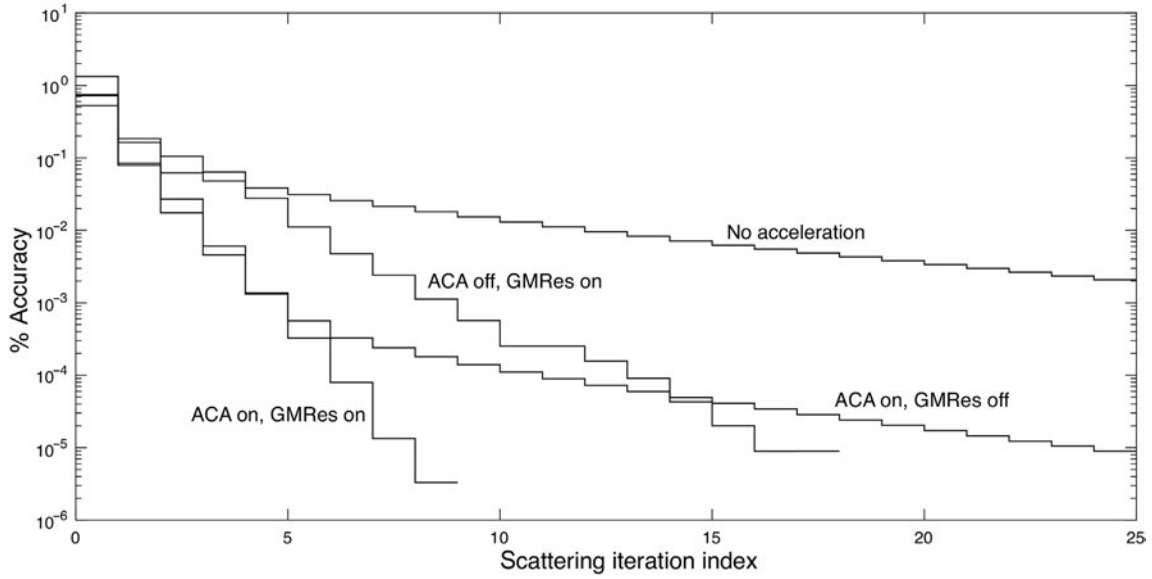

Fig. 5. Acceleration strategies for the MOC with LDC scheme. Linear scattering anisotropy is present. ACA, algebraic collapsing acceleration; GMRES, generalized minimal residual; LDC, linear discontinuous characteristics; MOC, method of characteristics.

boundary conditions). We have performed convergence studies relative to three variants of the method of characteristics, namely the SC and LDC schemes, and with respect to increasing mesh refinement of the original Cartesian mesh. Note that our implementation of the method of characteristics is also compatible with unstructured meshes.

Statistics will be given for k_{eff} and absorption rate distribution accuracies. In all tables, N_{tot} is the total number of unknowns per energy group. Memory requirements are proportional to N_{tot}, as no matrices need to be stored. In all cases studied, a reference solution was established from a spatially converged calculation. Reference absorption rates $R^*_{a,i}$ of assembly i were obtained with the following formula:

$$R^*_{\mathrm{a},i} = \frac{1}{V_i}\int_{V_i} d^3r[\Sigma(r) - \Sigma_{\mathrm{s}}(r)]\phi(r) \tag{36}$$

where $\Sigma_s(r)$ is the scattering cross section.

These reaction rates are then compared with data from less accurate calculations in order to obtain maximum $\varepsilon_{\max}$ and average $\overline{\varepsilon}$ errors.

3.1. The silver–indium–cadmium assembly benchmark

We investigated the application of the MOC in fundamental mode condition, focusing on specular boundary conditions

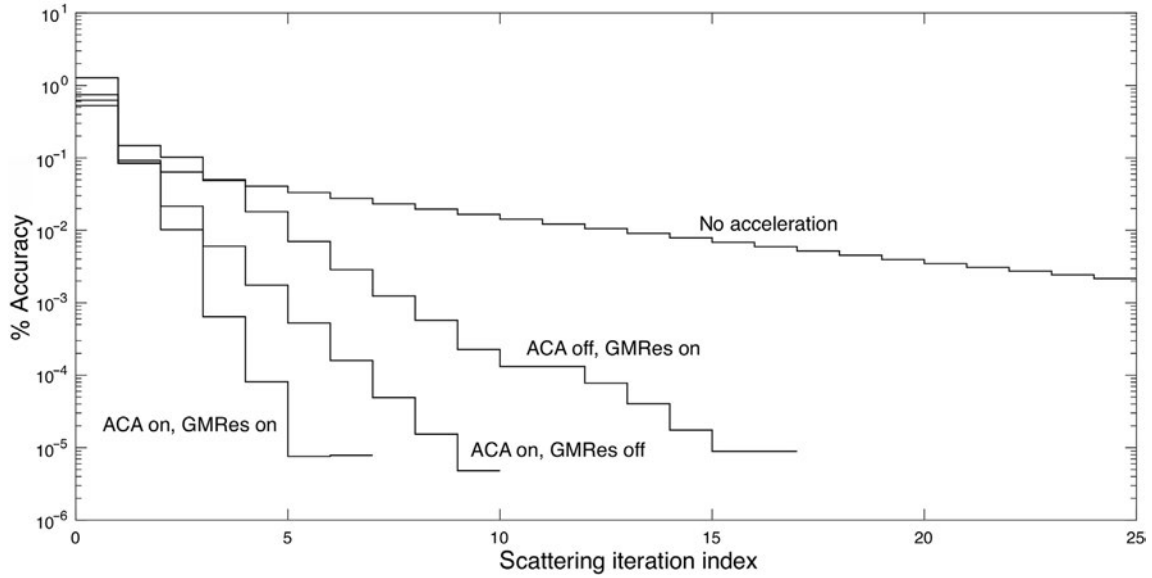

Fig. 6. Acceleration strategies for the MOC with SC scheme. Case with scattering isotropy. ACA, algebraic collapsing acceleration; GMRES, generalized minimal residual; MOC, method of characteristics; SC, step characteristics.

obtained with the introduction of cyclic characteristics. We have constructed a four-group Cartesian mockup of a production eight-symmetry PWR assembly with five silver–indium–cadmium (AIC) pins inserted. The corresponding geometry is depicted in Fig. 3. This benchmark retains many characteristics of a production assembly with more energy groups and with cylindrical pincells. The reactivity discrepancy between a P_0 and a P_1 scattering source is of the order of ~2380 pcm. This discrepancy is reduced to ~370 pcm if a transport correction is applied to the P_0 scattering source. Most lattice calculations are performed with a transport-corrected P_0 scattering source. In this case, an agreement with Monte Carlo better than 370 pcm is due to error compensation. This benchmark is therefore a good candidate for verifying both linear discontinuous and scattering anisotropy implementations of the neutrons sources in the MOC and for testing the effectiveness of the acceleration techniques.

The MOC method with SC and LDC schemes was implemented in DRAGON5 as described in the previous section. The SALT: module in DRAGON5 was used to generate a cyclic tracking with option “TSPC 12 25.0” set to select the number of planar angles and the number of tracks per cm. The cyclic tracks are computed on the eight-symmetry assembly, without unfolding the triangular domain. The reference solution is a DD2 approximation, with S_{18} level-symmetric quadrature and submesh $= 2 + 4$. (see Tables 1 and 2)

The implementation of ACA and GMRES(m) acceleration strategies were implemented in DRAGON5 as described in Section 3.10.3 of [1]. These strategies were applied to the four-group AIC benchmark in order to determine their effectiveness in the presence of scattering anisotropy and linear sources. The percent accuracy on the neutron flux in the fourth energy group is depicted in Figs. 4 and 5, corresponding to the step and linear discontinuous characteristic schemes, respectively. As expected, we observed a small decrease in effectiveness of the ACA method, if we compared Fig. 4 to Fig. 6 obtained for a case with scattering isotropy. The GMRES(m) effectiveness is not affected by scattering anisotropy and linear sources.

4. Conclusion

The implementation of the MOC in DRAGON5 is based on low and high order differencing schemes along finite or cyclic characteristics. Two foundation papers were dedicated to implementations of the MOC related to finite and cyclic characteristics, respectively [15,16]. This conference contribution completes the two foundation papers to cover issues related to acceleration of scattering iterations in the presence of scattering anisotropy and linear discontinuous sources. We have shown that acceleration techniques such as ACA and GMRES(m) remain effective in these conditions, in spite of a small decrease in ACA effectiveness. The resulting MOC implementation is therefore a candidate for performing accurate lattice calculations in a code similar to DRAGON5.

Conflicts of interest

The authors have no conflicts of interest to declare.

References

[1] A. Hébert, Applied Reactor Physics, second ed., Presses Internationales Polytechnique, Montréal, 2016, p. 396.
[2] J.R. Askew, A Characteristics Formulation of the Neutron Transport Equation in Complicated Geometries, Report AEEW-M 1108, United Kingdom Atomic Energy Establishment, Winfrith, 1972.
[3] M.J. Halsall, CACTUS, a Characteristics Solution to the Neutron Transport Equation in Complicated Geometries, Report AEEW-R 1291, United Kingdom Atomic Energy Establishment, Winfrith, 1980.
[4] I.R. Suslov, Solution of transport equation in 2- and 3-dimensional irregular geometry by the method of characteristics, in: Int. Conf. Math. Methods and Supercomputing in Nuclear Applications, Karlsruhe, April 19–23, 1993.
[5] R. Suslov, An improved transport theory scheme based on the quasi-stationary derivatives principle, in: Int. Conf. Math. Methods and Supercomputing for Nuclear Applications, Saratoga Springs, New York, October 5–9, 1997.
[6] R. Roy, The cyclic characteristics method, in: Int. Conf. Physics of Nuclear Science and Technology, Long Island, New York, October 5–8, 1998.
[7] R. Le Tellier, A. Hébert, On the integration scheme along a trajectory for the characteristics method, Ann. Nucl. Energy 33 (2006) 1260–1269.
[8] P.T. Petkov, T. Takeda, Transport calculations of MOX and UO2 pin cells by the method of characteristics, J. Nucl. Sci. Technol. 35 (1998) 874–885.
[9] S. Santandrea, R. Sanchez, Positive linear and nonlinear surface characteristic schemes for the neutron transport equation in unstructured geometries, in: Int. Conf. on the New Frontiers of Nuclear Technology: Reactor Physics, Safety and High-performance Computing. PHYSOR 2002, Seoul, October 2–10, 2002.
[10] S. Santandrea, R. Sanchez, P. Mosca, A linear surface characteristics approximation for neutron transport in unstructured meshes, Nucl. Sci. Eng. 160 (2008) 23–40.
[11] R.M. Ferrer, J.D. Rhodes III, Linear Source Approximation in CASMO5, PHYSOR 2012 Ð Advances in Reactor Physics—linking Research, Industry, and Education, Knoxville, Tennessee, USA, April 15–20, 2012.
[12] R.M. Ferrer, J.D. Rhodes III, Extension of Linear Source MOC methodology to Anisotropic Scattering in CASMO5, PHYSOR 2014—the Role of Reactor Physics toward a Sustainable Future, Kyoto, Japan, September 28–October 3, 2014.
[13] R.M. Ferrer, J.D. Rhodes III, A linear source approximation scheme for the method of characteristics, Nucl. Sci. Eng. 182 (2016) 151–165.
[14] G. Gunow, J. Tramm, B. Forget, K. Smith, Simple MOC—a Performance Abstraction for 3D MOC, MC2015—Joint International Conference on Mathematics and Computation (M&C), Supercomputing in Nuclear Applications (SNA) and the Monte Carlo (MC) Method, Nashville, Tennessee, April 19–23, 2015.
[15] A. Hébert, High-order diamond differencing along finite characteristics, Nucl. Sci. Eng. 169 (2011) 81–97.
[16] A. Hébert, High order linear discontinuous and diamond differencing schemes along cyclic characteristics, Nucl. Sci. Eng. 184 (2016) 591–603.
[17] A. Hébert, DRAGON5 and DONJON5, the contribution of École Polytechnique de Montréal to the SALOME platform, Ann. Nucl. Energy 87 (2016) 12–20.
[18] Y. Saad, M.H. Schultz, GMRES: a generalized minimal residual algorithm for solving nonsymmetric linear systems, SIAM J. Sci. Stat. Comput. 7 (1986) 856–869.
[19] R.E. Alcouffe, Diffusion synthetic acceleration methods for the diamond differenced discrete ordinates equations, Nucl. Sci. Eng. 64 (1977) 344–355.
[20] R. Le Tellier, A. Hébert, An improved algebraic collapsing acceleration with general boundary conditions for the characteristics method, Nucl. Sci. Eng. 156 (2007) 121–138.